

Dielectric Elastomer Actuators and Optical Character Recognition in a Braille Display

I. R. Botha^a, G. Bright^b, J. E. T. Collins^c

Received 15 March 2022, in revised form 19 August 2022 and accepted 26 August 2022

Abstract: The purpose of this study was the development and experimental validation of a novel portable tactile braille reading device. This design aimed to address the lack of quality braille reading material in South African schools dedicated to the blind and visually impaired. The design was divided into four subsystems: the actuation of the refreshable braille display, the mechanical design of the hand mounted device, the Optical Character Recognition (OCR) software and the electronic control system. The objectives of the study included the design of the electrical, mechanical and software subsystems of the device with emphasis on miniaturisation and a low-cost design, as well as the experimental validation of the haptic feedback and OCR subsystems. The system validation focussed on the experimental analysis of the OCR software design and the Dielectric Elastomer Actuators (DEAs) utilised in the refreshable display. The performance of low-cost elastomer and electrode materials were experimentally assessed during the design of the miniature DEAs. The ideal material combination for the proposed application was identified as a VHB4910 acrylic film lined with MG Chemicals 846 carbon grease. The largest vertical deflections of the diaphragm-type DEA were attained with a stipple-based electrode application, with the elastomer prestrained to 300 % initial area. The OCR program analysis indicated that multiple character recognition was more efficient and less prone to inaccuracies than the initially proposed single character recognition method. The integration of OCR software with miniature DEAs served as a novel approach to text-to-braille transcription.

Additional keywords: Dielectric elastomer actuators, optical character recognition, braille display, high-voltage control, Tesseract, Long-Short Term Memory

Nomenclature

Roman

A	Area [m ²]
C	Constant
E	Applied Electric Field [V/m]
V	Voltage [V]
t	Unit thickness [m]
Y	Elastic modulus [Pa]
s _t	Elastic compressive strain
a	Unactuated length [m]

r	Radius of curvature [m]
H	Convex height [m]

Greek

ϵ_r	Relative electric permittivity [F/m]
ϵ_0	Electric permittivity of free space [F/m]
δ	Induced strain in lateral/radial direction
θ	Angle of curvature [°]

1 Introduction

The global population of blind or visually impaired individuals was identified as approximately 253 million by the Orbis Annual Report [1]. The report further defined that 89 % of effected individuals live in low/middle income countries and that 75 % suffered from preventable or treatable conditions. Both statements prove true for a country such as South Africa where majority of the visually impaired population reside in remote areas and fall within the low-income bracket [2]. This economic position results in a limited access to treatment and a greater risk of developing malnutrition based visual impairments.

The next point to be considered is why 97 % of the blind and visually impaired population of South Africa is unemployed [3]. Life Healthcare states that the high unemployment rate is affected by the perception that the visually impaired cannot carry out daily tasks. This stigma is undoubtedly an issue in today's society; however, it also serves as a blanket statement to detract from a larger problem that highlights the education system's role in the precipitation of this stigma.

Therefore, the question of the high unemployment statistic must now be analysed in the scope of the education provided to blind and visually impaired students in South Africa. The primary challenges faced by the government in providing an equality-based educational system for the visually disabled can be grouped into four major areas: staff provisioning, adequate training of teachers, access to learner/teacher support material in braille, and access to assistive learning devices [4]. Khumalo & Fish-Hodgson asserts that a lack of an equitable budget dedicated to inclusive education at both a provincial and national level is a major opposition to overcoming these challenges.

The authors developed the following research question upon the assessment of the above challenges: "Can a Mechatronic design approach to portable text transcription provide a low-cost solution to the job accessibility crisis affecting the blind and visually impaired in South Africa?"

The device was required to be low cost to account for the socio-economic challenges of distribution in South Africa. The purpose of the device was to address the educational needs of school-age children. The lack of computers or funding for digital equipment introduced the additional requirement that the device be able to deal with the most common and inexpensive existing material, namely

- Discipline of Mechanical Engineering, University of KwaZulu-Natal, South Africa, bothai@ukzn.ac.za
- Discipline of Mechanical Engineering, University of KwaZulu-Natal, South Africa, brightg@ukzn.ac.za
- Department of Engineering, Bob Jones University, South Carolina, USA, jcollins@bju.edu

textbooks and printed subject matter provided by the Department of Education and public libraries. Further, the printed text was required to be transcribed into a medium accessible to the blind and visually impaired in real-time.

The objectives were achieved through the development and integration of four major subsystems: the actuation of the refreshable braille display, the mechanical design of the hand mounted device, the optical character recognition software and the electronic control system.

The primary research areas contributing to the development of the device included optical character recognition and dielectric elastomer technology. These two research areas comprised the input and output of the design respectively. The novel implementation of DEA technology as miniature actuators in a braille application is of particular interest. The paper provides a brief background on DEA technology and the relevant OCR application. Thereafter, the research method of the study is discussed, along with an overview of the design subsystems and experimental methodology employed. Findings and notable insights gained from the investigations are assessed and the report rounded off by a general design conclusion and recommendations.

2 Background

2.1 Dielectric elastomer actuators

Dielectric elastomer (DE) technology is a category of Electroactive Polymers (EAP) which act as actuators when in the presence of an electric field [5]. However, beyond the use as an actuator, DEs can also perform as generators or sensors should the relationship between actuation and electric field be reversed. This is due to DEs fundamentally operating as variable capacitors [6]. The DE consists of conformable electrodes layered on either side of an elastomer material. Therefore actuators, sensors and generators developed using this technology are highly deformable and particularly advantageous in applications that require miniaturisation or soft robotics. Before the working principle of DEAs are further discussed, it is beneficial to discuss how the advantages of DE actuator technology will benefit the specific application as a refreshable braille display.

The average dimensions of the dot base diameter and height are 1.44 mm and 0.48 mm respectively [7]. The tactile braille display will be mounted on the forefinger of the reader's hand to simulate the natural position when reading braille. The braille cell must conform to the finger and be as thin as possible as to not interfere with the proprioception of the reader [8]. In the case of reading braille, proprioception is centred around the pad of the index finger. Wu et al states that a minimum contact force of 50 mN at a minimum displacement of 0.25 mm is required to stimulate the shallowest mechanoreceptor [9]. The average reading rate of braille is approximately 120 words/min [10].

Commercially available refreshable braille display actuators are currently limited to piezo-bimorph technology. The drawback of these mechanisms is the module being comprised of auxiliary components attached to the pin, therefore limiting the minimum dimensions of the device, and increasing the risk of mechanical failure. Beyond placing limitations on miniaturisation, these drawbacks also result in

piezoelectric based braille displays being exorbitantly expensive [10]. The attraction of researching alternative actuation technology was primarily motivated by the reduction of these high costs as well as further miniaturisation of the design. The ideal actuator to be implemented in portable tactile displays were required to encompass the following properties: light weight design, low power, mass manufacturable and robust. All of which are qualities possessed by dielectric elastic actuators, the large strain potentials of DEAs are particularly attractive in comparison to alternative actuation technology.

2.2 Working principle of dielectric elastomer actuators

DEA technology depends on the elastic characteristics of the elastomer material to produce the necessary displacement. Consider a flat elastomer film sandwiched by two conformable elastomers of uniform size and shape. Upon the introduction of a voltage input to the electrodes, an electric field is induced. The resulting attraction experienced by the opposing electrode layers result in a decrease in thickness of the elastomeric material. Assuming the elastomer has the properties of an incompressible linearly elastic material of constant volume, the decrease in thickness results in an increase in area.

This reaction can be modelled mathematically using equation 1 through the implementation of the Maxwell stress equation to predict the theoretical elastic compressive strain of the DEA [11].

$$s_t = -\frac{\epsilon_r \epsilon_0 V^2}{\gamma t^2} \quad (1)$$

This paper is specifically based on a diaphragm-type DEA. The diaphragm design utilises rigid boundaries along the area of the electrodes to constrain the maximum lateral area expansion, figure 1(a) [12]. The constrained edges force the DEA to buckle and expand in a radial direction to maintain the constant volume of the elastomer. The upward deflection of the DEA generates the individual actuation required of the refreshable braille display.

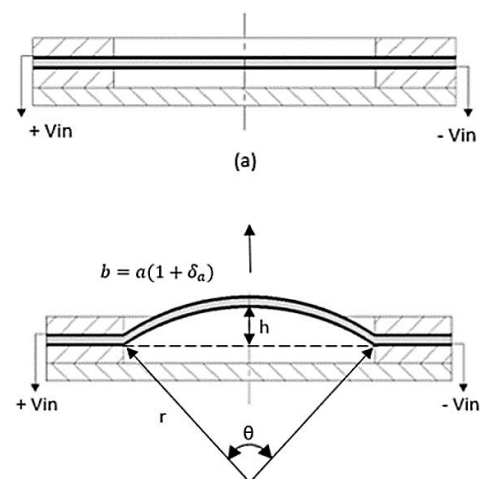


Figure 1 Actuation principle of tactile diaphragm-type DEA (a), with voltage input=0 (b), with voltage input ≠ 0

Consider equation 2 [13], which illustrates the calculated height that a diaphragm-type DEA will achieve. Equation 2

was determined through the application of strain calculation and the trigonometric properties of DEA illustrated in figure 1(b) to arrive at an approximation of the change in height. A detailed description of the equations can be found in the report published by Botha *et al.* [14].

$$h = \sqrt{\frac{(1-\delta_a)^3 a^2}{24\delta_a}} \left[1 - \cos\left(\frac{\sqrt{\frac{24\delta_a}{(1+\delta_a)}}}{2}\right) \right] \quad (2)$$

Another elastomeric property that neither equation 1 nor equation 2 consider is the impact of prestrain on material behaviour. Prestraining of elastomer films prior to voltage application has been attributed to the enhancement of dielectric breakdown strength [15]. However, the addition also introduces instabilities such as elastomeric creep and stress relaxation in the material [6]. Therefore, the effect of various percentages of prestrain and the combination of electrode and elastomer materials were assessed experimentally in this paper to determine the ideal candidate for the refreshable braille display.

2.3 Optical character recognition

Optical Character Recognition (OCR) refers to the process of extracting text data from images. OCR tasks that require data extraction from printed or typed text documents and images have several software packages available with popular choices being Tesseract, ABBYY FineReader, Adobe Acrobat Pro and OpenBook, TextCloner Pro and KNFB Reader [16,17]. Due to the commercial value of the abovementioned software, most limit the amount of customization available to the user. Of the listed packages, Tesseract is considered one of the most accurate open-source OCR engines currently available. Supporting operating systems include Mac, Windows and Linux [18]. Therefore, in a situation where a high level of function customization is required at low cost, Tesseract is the ideal solution.

Two versions of Tesseract are available for public use on Github: Tesseract 3 and 4 [19]. Tesseract 3 uses the Legacy OCR system to recognize character patterns by comparing each pattern to an existing library, this is an older version of Tesseract and is prone to errors. The more popular Tesseract 4 utilizes deep learning using the neural network; Long-Short Term Memory (LSTM) to complete more accurate character recognition [19].

Common strategies utilised by OCR software include matrix matching, fuzzy logic, feature extraction, structural analysis, and neural networks [18]. OCR Software pre-processes images to improve the ability to recognize the characters. This pre-processing consists of techniques such as [20]:

- De-skew (corrects alignment of page)
- Despeckle (smooth edges and removes positive and negative spots)
- Binarization (conversion to black and white image to lift useful data from background)
- Line removal (identifies columns, paragraphs, and sections as blocks)
- Zoning (divides words)
- Line and word detection (for multi-language documents)

- Segmentation
- Normalisation (normalize aspect ratio and scale)

Open-Source Computer Vision (OpenCV) is a library utilised for OCR which detects and defines text regions. OpenCV can be utilised to independently complete the text recognition tasks attributed to Tesseract, thus creating a standalone image capture and text recognition system without the need for Tesseract [21]. However, the development of the Tesseract software provides a concise platform for character recognition with numerous design iterations which have solved programming challenges that would need to be worked through again should OpenCV be used as a standalone program. It must be emphasised that only OpenCV can be used as a standalone OCR engine, Tesseract requires a secondary program like OpenCV or Leptonica to process the image before character recognition can be completed by Tesseract [22]. An advantage of using OpenCV independently for the task of text recognition over Tesseract would be in a situation where the text-to-braille design is expanded to include a variety of linguistic scripts, such as Tamil script [21]. This is because the Tesseract engine is currently limited to Latin script recognition. Upon consideration of the project aims, where a proof of concept of the mechanical design was priority, the OpenCV-Tesseract combination was ideal to reduce the time dedicated to programming and debugging. The online support available for OpenCV-Tesseract OCR text extraction was also a motivator for selecting this system due to its popularity amongst developers of prototype systems [23,24,25].

3 Research methods and design

3.1 Design overview

The methodology adopted during the development and design of the device took the form of an iterative process. Upon completion of the literature review, an agile design model was implemented. Subsystem design and testing were divided into three loops. A visual representation of the design development is illustrated in figure 2. Each loop commenced with the design of a subsystem, followed by the incorporation of a dependent subsystem. The dependent subsystem was tested, and the initial design then updated using the revised specifications or insights gained from the experimental results.

The assessment criteria of Stage 1 included the selection of the ideal elastomer and electrode materials to perform the study. The variable assessed during DEA material and synthesis testing was the percentage area strain achieved at different voltage inputs. The related mechanical design consisted of the portable finger mounting on which the DEA display and camera were to be mounted. The assessment criteria of Stage 2 included the performance accuracy and speed of the OCR software during the scanning of available printed text. The electronic design depended on both the specifications developed in Stage 1 and the performance of the OCR investigation. The final development stage included the final design of the tactile display and was based on the assessment criteria of the diaphragm proof-of-concept

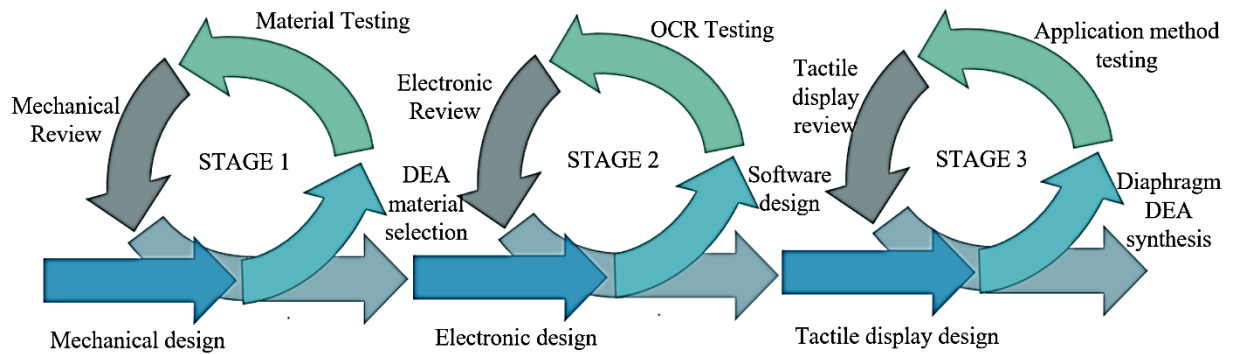


Figure 2 Design Model

experimental investigation. The performance of the diaphragm DEA was assessed according to the maximum vertical displacement achieved by the centre of the circular diaphragm at a range of voltage inputs.

The following sub-headings summarise the major design requirements of each subsystem and outline the proposed solution. The experimental methodology of the DEA material testing, OCR testing and diaphragm synthesis testing are then discussed

3.2 Mechanical design

For ease of reference, the authors elected to divide the mechanical design of the refreshable braille display into two sections. The actuator design is discussed under its own designated section due to the series of tests conducted on the dielectric elastomer system during manufacture. The second mechanical system consisted of the finger mounting and scanning hardware. The finger mounting, illustrated in the exploded view, figure 3, was required to house the scanning and actuation hardware of the device as well as meet the ergonomic requirements of the reader.

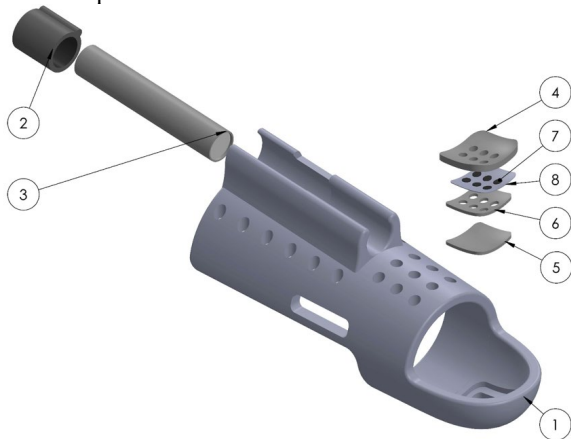


Figure 3 Exploded view of finger mounting subassembly

The 3D printed finger mounting was based on existing finger splint designs. Finger splint designs were selected due to the prioritisation of user comfort, particularly the interior contours of the mounting, while being robust enough to constrain the motion of the finger. The selected camera, represented as (3) in figure 3, was an endoscope with a minimum focal distance of 30 mm, chosen for its small, inobtrusive profile. In order to achieve the most accurate focal point of the camera and not shift between scanned lines

during reading, the camera should ideally be mounted on the medial phalanx of the index finger. The medial phalanx would allow for greater control of the focal point of the camera and prevent the risk of the camera straying to the preceding line of text should the reader adjust the angle of finger position. However, the position on the medial phalanx increases the cost and complexity of the camera to meet the required focal distance specifications. Therefore, by implementing a finger-brace design, a larger focal length was attained while maintaining the accuracy of line scanning, see figure 4. Areas A and B of figure 4 indicate the joints between the phalanges. By implementing a Velcro strap between the joints, the medial and proximal phalanges are constrained along the same axis of motion.

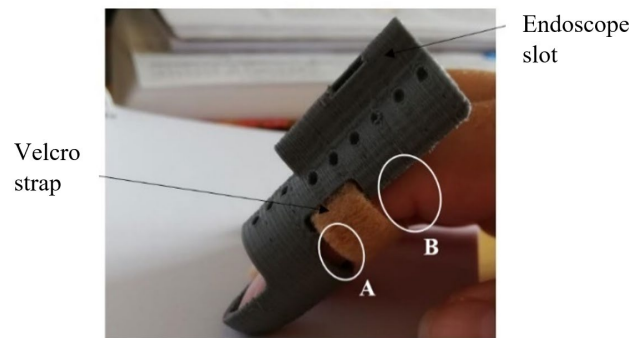


Figure 4 Photo of 3D printed prototype of finger mounting

3.3 Optical Character Recognition (OCR) software

According to the 2015 report by Russomanno et al. average braille reading speeds are approximately 120 words/min [10]. The proposed OCR sub-system transcribes each scanned text character to braille in real-time. Therefore, using the average reading speed stated above and the assumption of an average of 4.79 letters/word in the English language, a required reaction time of 0.418 s was calculated [26]. The authors used this value to analyse the performance of the OCR and determine if any adjustments to the design were required. Figure 5 illustrates the OCR procedure implemented in the design, with an endoscope as the input, DEA display the output and a Raspberry Pi Zero performing the OCR operations.

The Raspberry Pi Zero was configured to run both the Tesseract and OpenCV software and process scanned images. Once the character recognition was completed by Tesseract, the resultant ASCII code was converted to a braille equivalent

array of six voltage outputs via the GPIO pins. The complete code for this project can be found on Github [27].

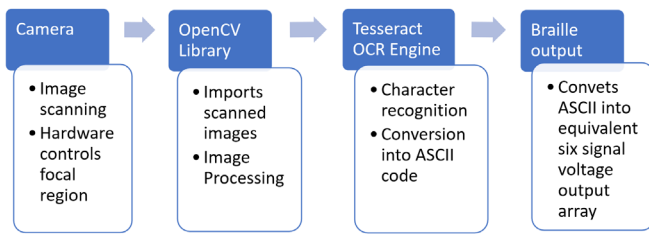


Figure 5 Optical character recognition procedure

A total of 5 experiments were run with the aim to test processing speed and accuracy of the OCR subsystem. In order to retain homogeneity within the tests, all test samples were arranged as the alphabet from A to Z. The variables that were changed were font, number of characters per sample, quality of scan image and lower case versus upper case.

Each image sample was uploaded to the OCR program. Thereafter, the code was run, and the processing time and output were recorded for analysis.

3.4 Electronic control system

Figure 6 illustrates a detailed schematic of the final electrical system implemented in the design. This subsystem was designed upon the analysis of the OCR and actuation requirements. All components were of the appropriate size to be arranged on the dorsal size of the hand, allowing for full wrist and finger mobility. Approximate weight of all components was 0.160 kg. The casing design of the electrical components and circuit were 3D printed. The complete prototype design is represented in figure 7.

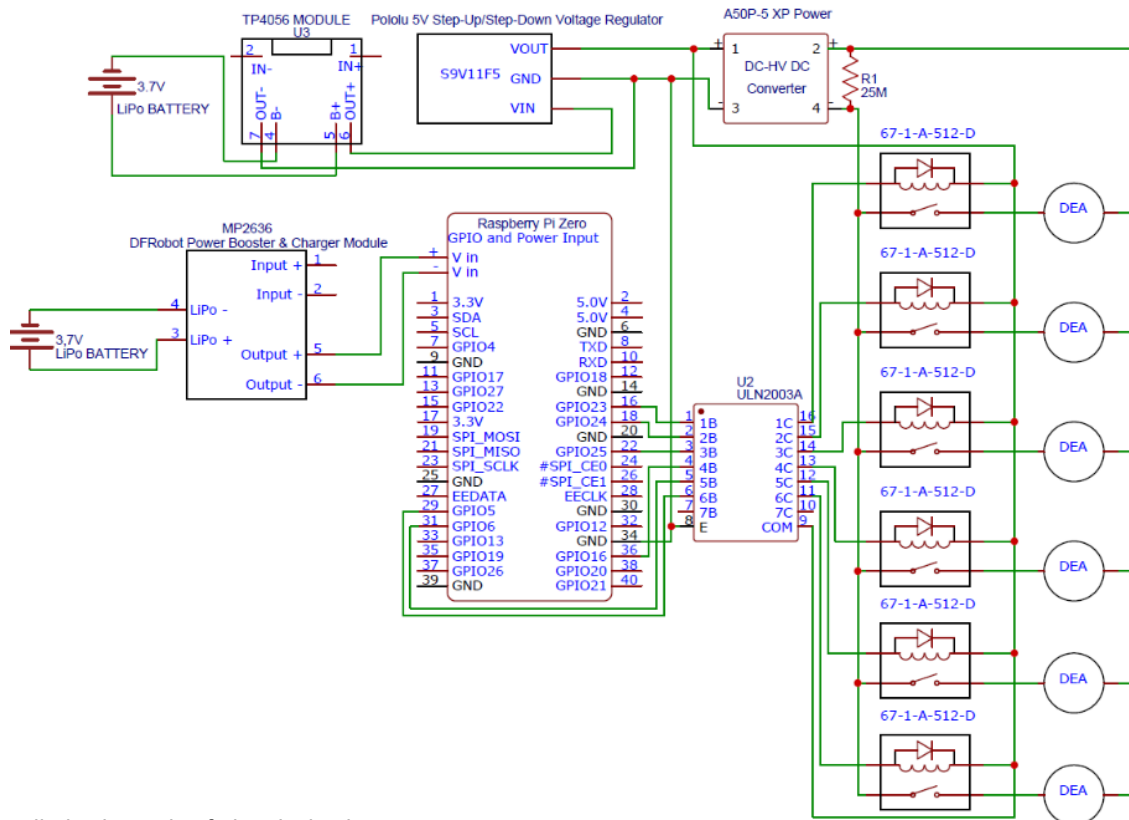


Figure 6 Detailed schematic of electrical sub-system

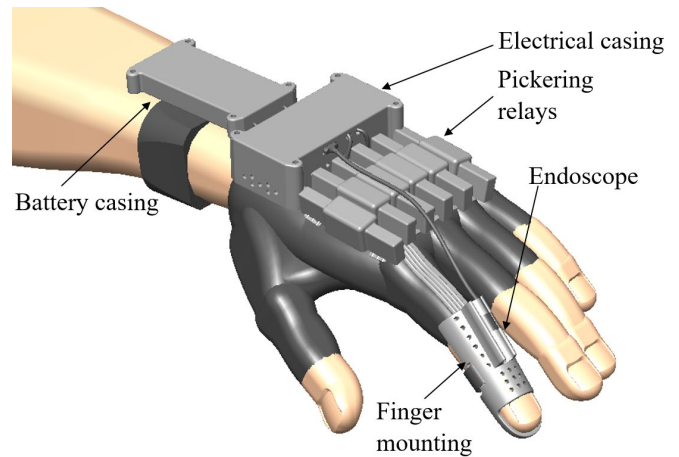


Figure 7 CAD model of prototype

One of the major drawbacks of DEA technology is the requirement for a high driving voltage. Literature indicates common voltage ranges of 500 V to 10 000 V [28], however, lower driving voltages have been researched through stacking multiple DEA layers to create an equivalent displacement [13]. Upon consideration of similar diaphragm-type applications, a maximum driving voltage of 5000 V was selected. Of course, this brings to question the portability and safety of the device.

Driving currents of DEAs are very low and, due to electrostatic properties, will only require power during area expansion [28]. Therefore, the low power requirements allowed the authors to implement a miniature DC to high voltage DC converter manufactured by XP EMCO. Two series were used during the design and manufacture of the

device, the G50 was used during proof-of-concept testing and material selection of the DEA and the A50 was designated as the series to be used in the final design. The A50P-5 series was selected due to its small frame of 28.69 x 6.35 x 11.43 mm and low input voltage of 5 V [29]. The rated power of the converter is 1 W, further ensuring the safety of the user along with its insulated casing.

In order to protect the sensitive circuitry of the Raspberry Pi Zero the high voltage side of the circuit was required to be isolated from the low voltage control side. This was achieved using six high voltage reed relays, specifically Pickering 67-1-A-5/2-D reed relays [30].

Two 3,7 V lithium polymer batteries were selected to power the prototype device. One of the batteries was connected solely to the Raspberry Pi via a power booster and charger module. This served to protect the Pi from possible voltage surge at the input side should the relays or the DC-HV DC converter be connected along the same circuit. The connection of the relays to an external power source further prevented the chance of the voltage spike on the output side of the Pi when a relay switch was de-energized.

It was further recommended by the Raspberry Pi manufacturers that only 3.3V signal logic be utilized at the output of the General-Purpose Input/Output (GPIO) pins [31]. The Pickering relays have a listed 'must operate voltage' of 3.75 V and a recommended voltage input of 5 V. This problem was circumvented by the introduction of ULN2003 Darlington transistor. The transistor made it possible to carry the required current of 125 mA per GPIO for the successful operation of the relay.

User safety was a priority during component selection and casing design, due to the placement along the dorsal side of the hand. Further, where current Li-Ion batteries are considerably cheaper than their Li-Po counterpart, Li-Po batteries maintain a more robust design, do not contain flammable solvents and avoid the risk of cell leakage [32]. The casings were designed with adequate ventilation in mind and allow for partitioned stacking of electronics to promote thermal regulation. The selection of encapsulated and fully sealed Pickering relays was vital to the design safety due to the high driving voltage [30]. Finally, all electrical components are mounted on the glove, and wrist band, preventing direct contact with the skin of the user. Snap fasteners held the electronics in place and also allowed for a modular design to cater for various hand sizes.

3.5 Tactile braille display

As indicated in figure 2, the design and analysis of the DEA tactile braille display was divided into two stages. The first iteration included the selection of the ideal electrode materials, elastomer material and percentage prestrain. The ideal combination was required to be low cost while achieving the greatest strain or area expansion results. Once the combination was selected, the materials were used to synthesise a proof-of-concept diaphragm-type DEA with the edges constrained to allow for out-of-plane displacement. The diaphragm-type DEA was a scaled-up proof-of-concept and was utilised to assess the effect of synthesis procedure and electrode application methodology on the performance of the DEA. Material selection was conducted using a study of total area expansion. The samples, as seen in figure 8, were

synthesised using laser cut Perspex frames. A camera was mounted above each sample and the area change was captured before and after voltage input. The data was then used to calculate the percentage area strain achieved by each sample.

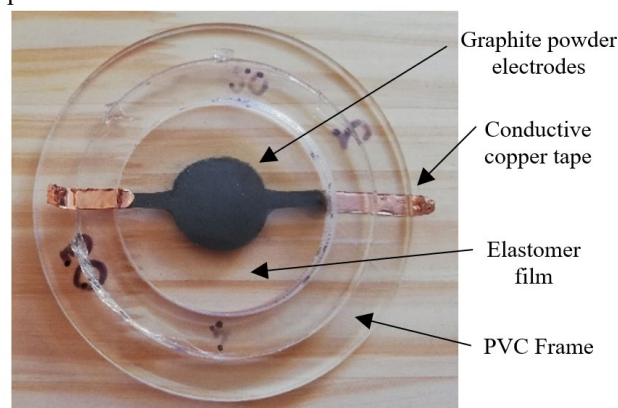


Figure 8 Photo of DEA sample used in strain test series [14]

The elastomer materials studied included the acrylic double sided adhesive films VHB4905 and VHB4910. The acrylic films had thicknesses of 0.5 mm and 1.0 mm respectively and were selected for the study based on previous literature indicating the superior efficiency, electric field generation, area strain, and maximum pressure when compared to other elastomer materials [28]. This study analysed the properties and response of VHB4910 and VHB4905 under various prestrain conditions. It was hypothesised that the VHB4905 would have superior results due to the smaller thickness, which agrees with the strain equation 1 where a reduction in thickness will result in a larger strain response.

Electrode materials to be assessed included two grades of graphite powder and a carbon grease. The first graphite powder was a common dry lubricant known as Pressol Powder, which was selected for its ease of application, low cost, and availability in South Africa [33]. This was to be compared to an internationally sourced brand known as Microfyne graphite powder lubricant. Microfyne exhibited a finer particle size of 44 μm and a carbon content of 95 % [34]. The authors hypothesised that the finer particle size would exhibit improved electrostatic properties, however, it was necessary to assess the degree of improved performance in conjunction with the cost and accessibility difference of the two powders. Should the results generate a strain difference that is negligible in light of the cost difference, then Pressol would be the preferred material. The carbon grease assessed in the experiment was a common carbon conductive grease known as MG Chemicals 846 [35]. During research of appropriate materials, it was observed that the matrix created by the grease resulted in multiple layers of particles being in contact at once. Therefore, upon expansion the layers of varying heights remain in contact and thus result in a constant layer on conductive material, whereas the powder samples consist of only a single layer adhered to the film. Therefore, upon expansion, the distance between particles increases and disrupt the homogenous conductivity of the electrode.

Once the materials were tested and an appropriate material combination selected, a proof-of-concept

diaphragm-type DEA was synthesised. The proof-of-concept was scaled to 13.88:1 of the actuators to be implemented in the braille display. This allowed for accurate data collection of the vertical deflection results. Two variations in synthesis procedure were experimentally assessed.

The first was the impact of electrode application on DEA performance. Three carbon grease electrode application methods were used; stippled, smeared diagonally, and smeared radially. The intention of the study was to assess the effect of non-homogenous application methods on DEA performance. The electrode material was applied to the elastomer after the film had been prestrained to 300% the original area on a large Perspex frame. A mask was applied to the area and the electrode material was applied to the surface using a cotton swab and the above-mentioned techniques. Smaller Perspex frames were then fixed to either side of the elastomer material in order to constrain to outer edges of the electrodes. Thereafter, a sealed cavity was created on one side of the DEA using a rubber gasket and Perspex base, figure 9. The sealed cavity was required in order to inflate the DEA and allow it to assume the initial diaphragm structure, illustrated in figure 10(b). The initial inflation of the DEA is considered as the introduction of a directional bias in the actuator, thus forcing the actuator to only produce a deflection response in the direction of the initial inflation.

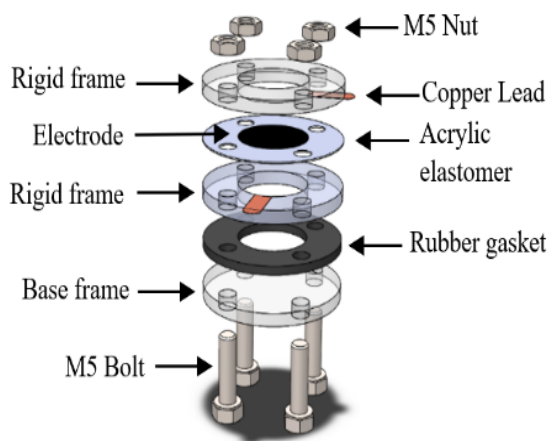


Figure 9 Exploded view of diaphragm DEA [12]

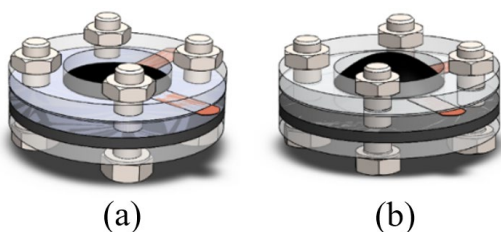


Figure 10 DEA assembly before and after inflation [12]

This directional bias was known as the initial height of the DEA and encompassed the second variation of synthesis procedure testing. The authors conducted multiple strain tests at various initial heights in order to assess the impact of initial height on the DEA performance. Section 4 of this paper details the results and findings of the investigations.

4 Findings and discussions

4.1 DEA material selection

Figures 11 through 13 are the graphical results generated from the first iteration of DEA testing. This series of experiments were conducted in order to select the ideal materials to be implemented in the second iteration of diaphragm proof-of-concept testing.

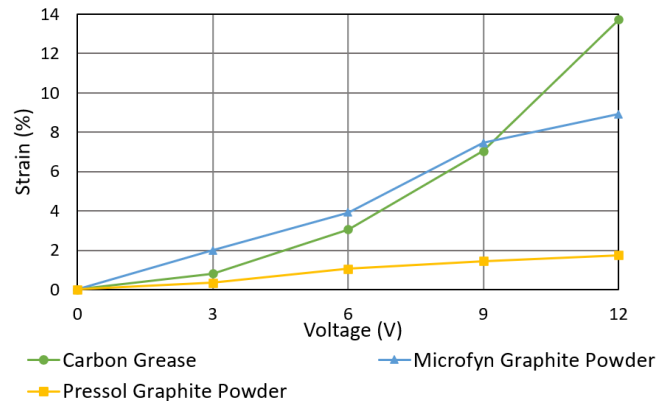


Figure 11 Effect of electrode material selection on DEA strain performance

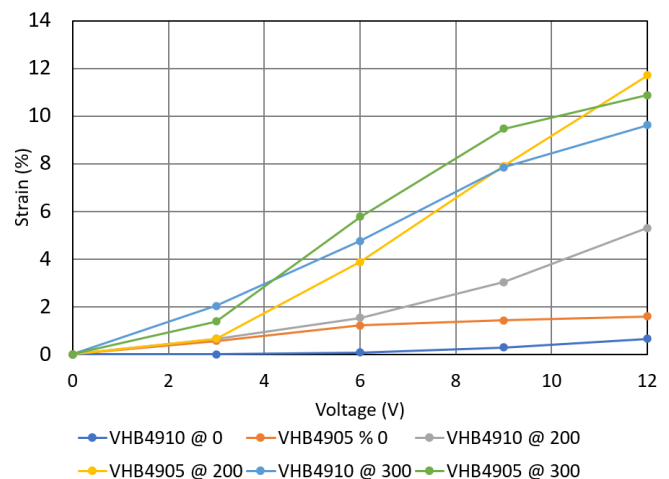


Figure 12 Effect of elastomer prestrain on DEA strain performance [14]

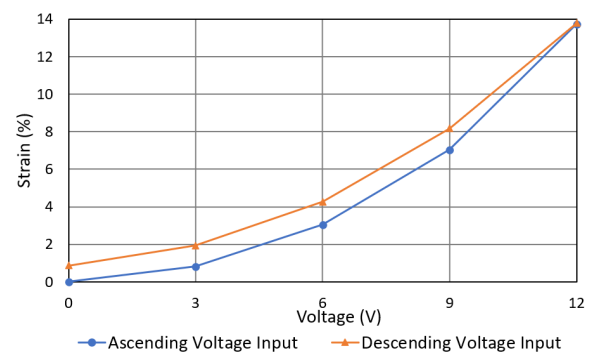


Figure 13 Effect of ascending versus descending voltage input during DEA actuation [14]

The Microfyn and Pressol curves in figure 11 confirmed the original hypothesis that the finer grade particulate of graphite exhibited superior strain properties than the less expensive Pressol grade material. The largest strain results were achieved by the carbon grease electrode samples, agreeing with the author assumption that particles suspended in a matrix will generate improved electrostatic properties than a powder adhered directly to the surface of the elastomer film.

The information represented in figure 12 assessed two variables: the impact of prestrain on the strain and the performance of two elastomer materials (VHB 4910 and VHB 4905). The thinner elastomer film (VHB 4905) exceeded the performance of VHB 4910 at all prestrain percentages. However, even though VHB 4905 generated the largest strain results at 200% and 300% prestrain, a greater volatility was observed at 12 V input. The averages of three samples of each combination were used to plot the curves, and the VHB 4905 presented a high failure rate under repeated testing at 200% and 300% prestrain at maximum voltage. Therefore, even though successful samples of the VHB 4905 produced maximum strain results, the impact of high prestrain percentages on the thinner film introduced electromechanical instability and mechanical rupture. Upon consideration of these results, the authors elected to select the more stable VHB 4910 at 300 % prestrain as the final material combination. It must be noted that the test conducted in figure 12 used the Microfyn powder as the electrode. Therefore, the final selected material combination of carbon grease, VHB4910 acrylic and 300 % prestrain generated an average maximum strain of 13.75 %, as seen on figure 11.

A final area strain test was conducted to compare the strain results when results were taken in ascending intervals from 0 V to 12 V and descending intervals from 12 V to 0 V. The resultant graph, figure 13, indicated that the capacitive properties of the DEA was resulting in a degree of energy storage which therefore resulted in a skewed descending interval curve. This resulted in a final displacement of greater than 0 mm even when there was no voltage supply. Such displacement inaccuracies will impact strain-sensitive applications and if samples undergo repeated loading within a short space of time. A suggested solution was to increase the resistance of the bleeder resistor positioned in parallel to the output. This will assist in draining the remaining charge from the DEA.

4.2 Diaphragm-type DEA performance

Once the ideal material combination was selected, the diaphragm-shaped proof-of-concept samples were synthesised to assess electrode application techniques, and the impact of initial inflation heights. The graphs illustrated in figures 14 through 17 present the results of the experimental analysis.

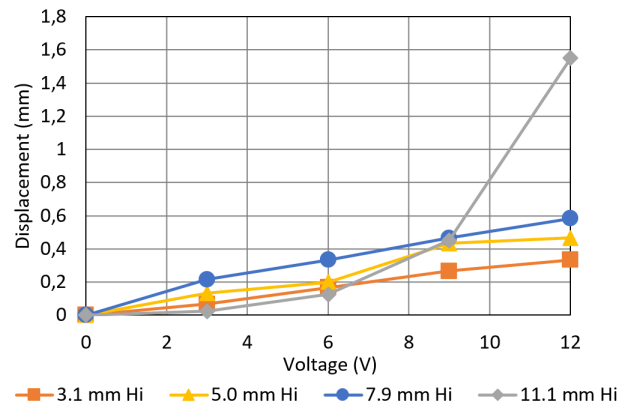


Figure 14 Vertical displacement of DEA with stippled electrode application at various initial heights (Hi) versus input voltage [12]

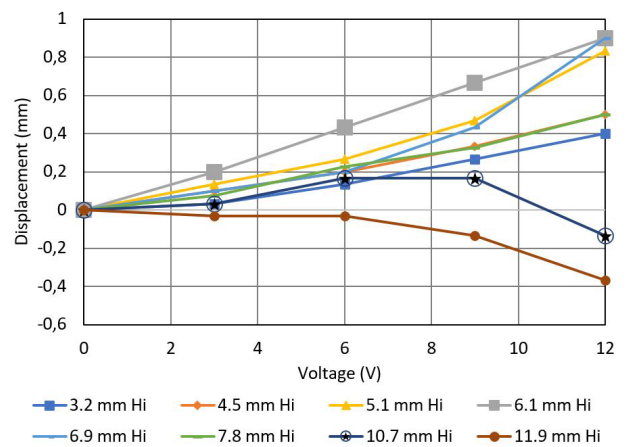


Figure 15 Vertical displacement of DEA with diagonally smeared electrode application at various initial heights (Hi) versus input voltage [12]

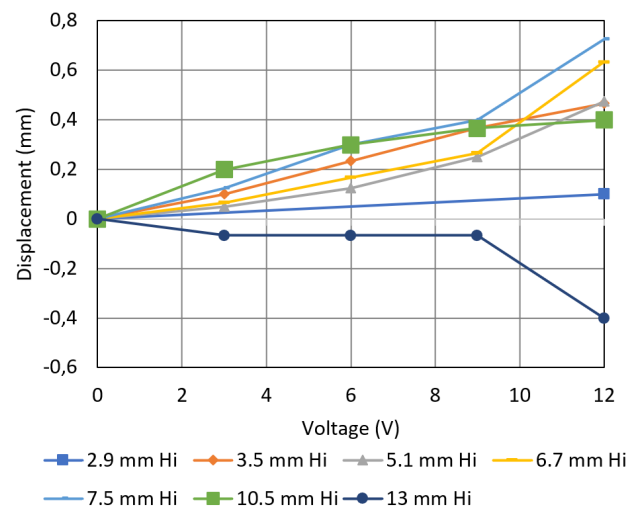


Figure 16 Vertical displacement of DEA with radially smeared electrode application at various initial heights (Hi) versus input voltage [12]

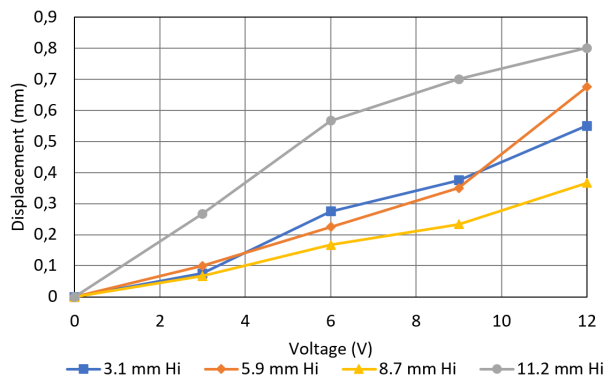


Figure 17 Vertical displacement of stippled and sealed DEA at various initial heights (Hi) versus input voltage [12]

All samples at small initial heights performed as hypothesised where an increase in initial height resulted in an increase in vertical displacement. However, as the initial heights increased beyond approximately 6 mm the application methods proceeded to modify the strain behaviour and direction. The samples prepared using the stipple method experienced an exponential increase in vertical strain at initial heights greater than 6 mm, while both the radially and diagonally smeared samples continued to expand but in the latitudinal direction, as indicated in figure 14, figure 15 and figure 16. Therefore, the largest vertical strain was achieved by the stippled samples at an average initial height of 11.1 mm.

A series of sealed stippled samples were also synthesised to assess the impact of a second acrylic film adhered to the surface of the DEA as a protective film. The protective film resulted in a drop of maximum vertical displacement to 0.8 mm. However, advantages of the protective film observed in figure 17 include the stabilising effect the film had on the strain curves, thus preventing exponential increases at high initial heights and preventing electromechanical instability.

4.3 Optical character recognition software performance

The optical character recognition software was analyzed in parallel with the final diaphragm DEA tests. Therefore, the scanned results were presented as printed output and an LED

3x2 matrix which supplemented the DEA response. This was necessary since the DEA actuators were still under development at time of OCR testing. Table 1 summarizes the processing speed and percentage accuracy of the different Font and character sequence samples with all pre-processing functions activated. The accuracy was calculated as a percentage of characters correctly identified for each test sample.

Table 1 Response time and average accuracy of different fonts during OCR Testing

Multiple/Single Character Image	Font	Response Time (s)	Average Accuracy
Multiple	Ariel	7.016	100 %
Multiple	Serif	6.875	3.846 %
Multiple	Typewriter	9.162	88.46 %
Multiple	Times New Roman	6.953	100 %
All multiple character samples		7.501	73 %
Single	Ariel	5.696	84.62 %
Single	Serif	5.629	84.62 %
Single	Typewriter	5.781	34.62 %
Single	Times New Roman	5.663	80.77 %
All single character samples		5.692	71.16 %

Beyond the results indicated in table 1, three lower case tests samples were also analysed to compare performance to the uppercase OCR results. Two of the samples contained multiple characters and were in fonts Ariel and Times New Roman, both produced an average accuracy of 100 % and response times of 6.599 s and 7.117 s respectively. The single character lower case test batch was in the Ariel font and produced an average accuracy of 38.46 % and an average response time of 5.638 s. Therefore, it was concluded that the performance of the OCR when recognizing multiple characters in either upper or lower case remains consistent, however, the accuracy of recognizing single lowercase characters reduced by 45.24 %.

Table 1 indicated that the average response time required to perform OCR of a single character was measured as 5.692 s. This far exceeded the required response time of maximum 0.418 seconds. In comparison, the multiple character samples (26 letters of the alphabet) produced an average response time of 7.501 s, therefore 0.288 s per character. Two possible solutions to the single character response time are discussed below.

Table 2 Accuracy and response time of multiple character OCR testing

Font	Ariel		Serif		Typewriter		Times New Roman	
Description	Accuracy (%)	Response Time (s)	Accuracy (%)	Response Time (s)	Accuracy (%)	Response Time (s)	Accuracy (%)	Response Time (s)
All activated	100	7.0157	3.846	6.875	88.46	9.162	100	6.953
Line-removal deactivated	100	6.975	3.846	6.843	88.46	9.143	100	7.009
All pre-processing deactivated	100	4.734	3.846	4.438	76.92	4.772	100	4.724
PSM configured to 3	100	7.031	3.846	6.858	88.46	9.173	100	7.061
Blur deactivated	100	4.286	3.846	4.203	76.92	4.586	100	4.356
Gray deactivated	100	8.108	3.846	8.291	76.92	9.732	100	8.297
Image Resize deactivated	100	12.091	3.846	7.382	92.31	7.764	100	9.398
Average	100	7.177	3.846	6.413	84.064	7.762	100	6.828
Variance	0	5.633	0	1.978	39.869	4.109	0	1.829
Standard Deviation	0	2.373	0	1.406	6.314	2.027	0	1.352

The first proposed solution is the implementation of a Raspberry Pi model possessing a processing speed greater than 1 GHz and a Random-Access Memory (RAM) exceeding 512 MB. This will drastically improve performance; however, it will come at the cost of a larger design footprint that will impact the portability of the device. An alternative solution is the scanning of sections of text at a time instead of single characters. This option will also ensure a higher OCR accuracy. Once the section of text is scanned, the user can still simulate the action of reading traditional braille by moving their finger across the page, without the chance of inaccurate braille output.

The variance and standard deviation of the results presented in table 1 were calculated to assess the reliability of the OCR program. The software response time standard deviation was calculated to be 0.0223 s for multiple character samples and 0.0565 s for single character samples. Considering the average response time for multiple and single character samples were 7.501 s and 5.692 s, respectively, the magnitude of the standard deviation to the 10^{-2} power indicated a negligible variance between the results and the average performance. However, the standard deviation observed for the accuracy of the software displayed larger margins of error. A standard deviation of 40.245 % was calculated for all multiple character samples. This was a result of the notably low accuracy of 3.846 % when the Serif font multiple character sample was processed by the program. Similarly, the Typewriter font delivered a lower accuracy of 34.62 % for the single character samples. In the case of the multiple character samples, the Serif font was chosen specifically for its structural divergence from the Arial and Cambria fonts which is known to perform best when sampled by the Tesseract OCR. According to the test data, the primary reason for the poor recognition performance of the Typewriter font single characters was the image resize pre-processing function. The performance improved for 12 out of the 27 letters when image resize was deactivated. In conclusion, the increase in resolution and the Dots Per Inch (DPI) of the images was decreasing the accuracy of the image recognition. A possible solution is to include an auto-scale command in the code, which assesses the DPI of the existing image before rescaling to 620 by 480 pixels. Another possible reason for the poor performance of the image rescale command was the set pixel dimensions which resulted in distortion of the original image. A possible solution would be to replace the existing rescale command to scale up the image using a set f_x and f_y value instead of distorting the image to fit the exact 620x480 pixel resolution [36].

Further testing was completed on the impact of pre-processing, line-removal and PSM specification on the multiple character sample sets. Table 2 summarises the results of these experiments.

Table 2 indicated that the pre-processing was most useful in scenarios where the original character quality was reduced e.g., the typewriter text sample. Line removal had a marginal impact on processing time, however, the 10^{-1} ms effect did not sufficiently support the deactivation of the line-removal operation when compared to the advantages of remaining active. The deactivation of image resize increased the length of processing time of multiple character images, an interesting observation since the opposite was observed in

single character recognition. It was further noted that the deactivation of image resizing not only increased accuracy of most single character tests but also reduced the total processing time.

When considering the standard deviation of the results in table 2, the performance percentage deviation was considered marginal; however, notable variances were observed for the response time. The largest standard deviation recorded for response time was for the Ariel font samples. Since the results of the Ariel samples indicated that the accuracy would remain at 100 % regardless of pre-processing functions, it could be concluded that pre-processing can be disabled for the sake of a faster response time. However, as indicated by the results of the Typewriter font, pre-processing is necessary to maintain the integrity of more structurally variant fonts. Since the device is intended for use on a wide range of printed mediums, the deviation in response time is a necessary sacrifice to maintain the accuracy of the OCR subsystem.

5 Conclusions and recommendations

The aim of the research was to investigate, design and analyse the viability of a portable, low-cost text-to-braille transcription device as a solution to the lack of accessible information available to the visually impaired. The success and operation of the design was assessed through a series of three experimental evaluations which highlighted the research contribution of the authors.

Area one of testing included the OCR software used to transcribe the scanned text to a six-array braille output. The programme consisted of the OCR engines OpenCV and Tesseract and were set up on a Raspberry Pi Zero. The purpose of the analysis was to determine if the Tesseract-OpenCV OCR met the criteria of the device, particularly the processing time required to match the average reading speed of a braille reader. The results disproved the hypothesis that single character OCR would require a shorter processing time than an image containing multiple characters. Of course, it was possible to increase single character OCR by selecting a microcomputer with a greater processing speed and RAM capabilities. However, this would come at the cost of decreased portability since the Raspberry Pi Zero was specifically selected for its size and weight. Therefore, it was preferable to retain the abovementioned microcomputer by adjusting the system to instead process multiple lines of text at once and then allow the reader to read the segment using the braille display before scanning the next section of the page.

The remaining two areas of testing included the experimental investigation of the ideal synthesis method and structure of the DEA to achieve the required vertical strain while maintaining the dimensional requirements of a traditional braille cell. This was accomplished through a series of iterative experiments. The first set explored the synthesis of the DEA braille cell using various low-cost materials. Once appropriate materials were selected, the second set of experiments examined the performance of the final proof of concept. The ideal combination of materials was determined to be a VHB 4910 film prestrained to 300 % the original area and lined with carbon grease electrodes. This

combination also satisfied the low-cost requirement of the design.

The second iteration of DE testing assessed the performance of diaphragm-shaped DEAs and the impact of different synthesis techniques. The best performing synthesis technique included a stippled application of carbon grease with an initial height of 11.1 mm. This technique resulted in a maximum vertical displacement of 1.6 mm. Once the scale ratio was applied, the stippled results would produce a predicted maximum displacement of 0.115 mm. This did not meet the required nominal braille dot height of 0.25 mm to stimulate the shallowest mechanoreceptor. Therefore, even though a low-cost solution to a refreshable braille display was developed, further research is required to achieve the required vertical displacement. Future research includes the investigation of the structural changes to the diaphragm DEA synthesis to achieve an increased actuated height. This includes alternative elastomer materials with properties that allow for the stacking of multiple layers. Alternative electrode materials can also be explored; however, this should be limited to circumstances in which the aim of the project is not dependent on a low-cost design. Electrode materials such as Ketjenblack [37] will provide improved performance but are significantly more expensive than the materials used in this research project.

6 Acknowledgements

This work is based on the research supported in part by the National Research Foundation of South Africa (Scarce Skills Masters Block Grant).

References

- [1] ISSUU. Orbis 2018 Annual Report. URL https://issuu.com/orbisintl/docs/2018_annual_report_digital_copy, 2018.
- [2] J. D. Steinmetz., et al. Causes of blindness and vision impairment in 2020 and trends over 30 years: evaluating the prevalence of avoidable blindness in relation to VISION 2020: the Right to Sight. *Lancet Global Health*, 9(2):144-160, 2020.
- [3] Life Healthcare tackles biggest disability in the country. URL <https://www.lifehealthcare.co.za/news-and-info-hub/latest-news/life-healthcare-tackles-biggest-disability-in-the-country/>.
- [4] S. Khumalo and T. Fish-Hodgson. Left in the dark: Failure to provide access to quality education to blind and partially sighted individuals in South Africa. *Section27*, Johannesburg, 2016.
- [5] Y. Bar-Cohen. Electroactive, Polymer (EAP) Actuators as Artificial Muscle. *Potential and Challenges*, 98, 2004.
- [6] L. Romasanta, M. Lopez-Manchado and R. Verdejo. Increasing the performance of dielectric elastomer actuators: A review from the materials perspective. *Progress in Polymer Science*, 51:188-211, 2015.
- [7] National Library Service for the Blind and Physically Handicapped of the Library of Congress. Section 3.2 of Specification 800 (Braille Books and Pamphlets), United States, 2008.
- [8] National Federation of the Blind. The Braille Literacy Crisis in America. National Federation of the Blind, Jernigan Institute, 2009.
- [9] X. Wu, H. Zhu, S.-H. Kim and M. G. Allen. A Portable Pneumatically-actuated Refreshable Braille Cell. *TRANSDUCERS 2007-2007 International Solid-State Sensors, Actuators and Microsystems Conference*. IEEE, pp. 1409-1412, 2007.
- [10] A. Russomanno, S. O'Modhrain, B. Gillespie and M. Rodger. Refreshing Refreshable Braille Displays. *IEEE Transactions on Haptics*, 8(3):287-297, 2015.
- [11] R. E. Pelrine, R. D. Kornbluh and J. P. Joseph. Electrostriction of polymer dielectrics with compliant electrodes as a means of actuation. *Sensors and Actuators A: Physical*, 64(1):77-85, 1998.
- [12] I. R. Botha, G. Bright and J. E. T. Collins. Impact of the Synthesis Procedure of Diaphragm-Shaped Dielectric Elastomers on the Performance as Novel Miniature Actuators. *International Conference on Electrical, Control and Instrumentation Engineering (ICECIE)*, Kuala Lumpur, Malaysia, 2021.
- [13] I. Koo, K. Jung, J. Koo, Y. Lee, and H. Choi. Wearable Tactile Display Based on Soft Actuator. *IEEE International Conference on Robotics and Automation*, Florida, pp 2220-2225, 2006.
- [14] I. Botha, G. Bright and J. Collins. Evaluation of Dielectric Elastomers in Applications as Low Cost, Small-Scale Actuators. *International SAUPEC/ROBMECH/PRASA Conference*, Cape Town, South Africa, 2020.
- [15] M. Kumar, A. Sharma, S. Hait, S. Wießner, G. Heinrich, I. Arief, K. Naskar, K. W. Stöckelhuber and A. Das. Effect of prestrain on the actuation characteristics of dielectric elastomers. *Polymers*, 12(11):2694, 2020.
- [16] Illinois Library. Introduction to OCR and Searchable PDFs: An Introduction to OCR. URL <https://guides.library.illinois.edu/OCR>, 2019. [Accessed 02 June 2020].
- [17] American Foundation for the Blind. Optical Character Recognition Systems. American Foundation for the Blind, URL <https://www.afb.org/node/16207/optical-character-recognition-systems>.
- [18] Tesseract-ocr. URL <https://github.com/tesseract-ocr/tesseract>, 2020.
- [19] R. Smith. An Overview of the Tesseract OCR Engine. URL <https://static.googleusercontent.com/media/research.google.com/en/pubs/archive/33418.pdf>.
- [20] F. Karandish. The Comprehensive Guide to Optical Character Recognition (OCR). MOOVAI, URL <https://moov.ai/en/blog/optical-character-recognition-ocr/>, 2019.
- [21] V. A. Devi and S. S. Baboo. Embedded Optical Character Recognition on Tamil Text Image Using Raspberry Pi. *International Journal of Computer Science Trends and Technology*, 2(4):11-15, 2014.
- [22] Tesseract-OCR. Tesseract Documentation, URL <https://tesseract-ocr.github.io/tessdoc/ImproveQuality>.

- [23] E. Ehiorobo. Basic OCR with Tesseract and OpenCV. URL <https://medium.com/building-a-simple-text-correction-tool/basic-ocr-with-tesseract-and-opencv-34fae6ab3400>, 2019.
- [24] T. Tran. [C++] Extracting Text from Image with OpenCV and Tesseract. *Machine Talk*, URL <https://machinetalk.org/2020/03/23/c-extracting-text-from-image-with-opencv-and-tesseract/>, 2020.
- [25] V. S. Chandel. Deep Learning based Text Recognition (OCR) using Tesseract and OpenCV. *LearnOpenCV*, URL <https://www.learnopencv.com/deep-learning-based-text-recognition-ocr-using-tesseract-and-opencv/>, 2018.
- [26] P. Norvig. English Letter Frequency Counts: Mayzner Revisited. URL <http://norvig.com/mayzner.html>, 2012.
- [27] I. Botha. Github OCR-Braille-Code repository. URL <https://github.com/Ingrid-B/OCR-BRAILLE-CODE>, 2021.
- [28] P. Brochu and Q. Pei. Advances in Dielectric Elastomers for Actuators and Artificial Muscles. *Macromolecular Rapid Communication*, 31:10-36, 2010.
- [29] XP Power. A Series DC-HVDC Converter. URL https://www.xppower.com/portals/0/pdfs/SF_A_Series.pdf, 2020.
- [30] Pickering. High Voltage Dry Reed Relays Pickering Series 67.68. URL <https://www.pickeringrelay.com/pdfs/67-68-high-voltage-reed-relays.pdf>, 2020.
- [31] General Purpose Input/Output pins on the Raspberry Pi. Raspberry Pi. URL <https://www.raspberrypi.org/documentation/hardware/raspberrypi/gpio/README.md>, 2020.
- [32] J. Kalhoff, G. G. Eshetu, D. Bresser and S. Passerini. Safer Electrolytes for Lithium-Ion Batteries: State of the Art and Perspectives. *ChemSusChem*, 8(13):2154-2175, 2015.
- [33] RS Pro. Pressol Lubricant 50 g Graphite Bottle. RS Components, URL <https://za.rs-online.com/web/p/lubricants/7031086/>.
- [34] Amazon. Microfyne Graphite Powder Lubricant, 12oz can. URL https://www.amazon.com/Microfyne-Graphite-Powder-Lubricant-12oz/dp/B079X4LK36/ref=sr_1_1?crid=2D5JNRUD6XMA0&keywords=microfyne+graphite&qid=1570649391&prefix=microfyn%2Caps%2C606&sr=8-1.
- [35] Amazon. MG Chemicals Carbon Conductive Grease, 80g Tube. URL https://www.amazon.com/gp/product/B005T8ROWA/ref=ppx_yo_dt_b_asin_title_o00_s00?ie=UTF8&psc=1.
- [36] K. Kuguoglu. How to use image preprocessing to improve the accuracy of Tesseract. freeCodeCamp. URL <https://medium.com/free-code-camp/getting-started-with-tesseract-part-ii-f7f9a0899b3f>, 2018.
- [37] Akzo Nobel Chemicals. Ketjenblack EC-300J Specification Sheet. URL <https://www.fuelcellstore.com/spec-sheets/ketjenblack-ec-300j-fact-sheet.pdf>, 2020.